Journal of Zhejiang University-SCIENCE B 2026 27(6):628-644
www.jzus.zju.edu.cn; www.springer.com/journal/11585
E-mail: jzus_b@zju.edu.cn

Research Article
https://doi.org/10.1631/jzus.B2400611

Regenerative potential of Schneiderian membrane-derived mesenchymal stem cells in sinus floor elevation model and calvarial defect model

Yuxin ZHAO*, Jia WANG*, Dongqi YOU, Yifan LU, Mengfei YU✉, Misi SI✉

Stomatology Hospital, School of Stomatology, Zhejiang University School of Medicine, Zhejiang Provincial Clinical Research Center for Oral Diseases, Key Laboratory of Oral Biomedical Research of Zhejiang Province, Cancer Center of Zhejiang University, Engineering Research Center of Oral Biomaterials and Devices of Zhejiang Province, Hangzhou 310000, China

Abstract: Objectives: Schneiderian membrane-derived mesenchymal stem cells (SMMSCs) have been reported to be osteogenic progenitor cells in vitro. However, there is controversy regarding the intrinsic osteogenic capacity of the Schneiderian membrane, and the bone formation potential of SMMSCs in vivo has never been reported. Therefore, in this study, we aimed to evaluate the contribution of the Schneiderian membrane to sinus floor elevation and to verify the function of SMMSCs in cranial bone defects. Materials and methods: Bilateral sinus floor elevation with chloromethyl-benzamidodialkylcarbocyanine (CM-Dil) labeling was performed in rabbits to assess Schneiderian membrane osteogenesis. Single-cell RNA sequencing was used to characterize human Schneiderian membrane cellular subsets. SMMSCs and bone marrow-derived mesenchymal stem cells (BMSCs) were transplanted into rabbit cranial defects with gelatin methacryloyl (GelMA) scaffolds and analyzed via micro-computed tomography (micro-CT) and histology. Results: Spontaneous bone formation adjacent to the Schneiderian membrane was observed. Single-cell analysis identified paired-related homeobox 1 (*PRRX1*) progenitor clusters driving endosinus osteogenesis. SMMSCs exhibited earlier and superior bone regeneration compared with BMSCs, with higher tissue volume and bone volume/total volume (BV/TV) ratios at four weeks after surgery. Conclusions: The Schneiderian membrane likely contributes to osteogenesis via *PRRX1*$^+$ progenitor lineages. SMMSCs promote accelerated early bone regeneration in cranial defects. This study provides the first in vivo validation of the osteogenic capacity of SMMSCs and defines their molecular identity at single-cell resolution.

Key words: Schneiderian membrane-derived mesenchymal stem cells (SMMSCs); Single-cell RNA sequencing; Osteogenesis; Maxillary sinus floor elevation (MSFE); Calvarial defect

1 Introduction

Owing to the insufficient bone height and poor bone quality in the maxillary posterior region, the placement of dental implants is often challenging, and the maxillary sinus floor elevation (MSFE) procedure has been widely performed by clinicians to solve this problem (Tatum, 1986; Summers, 1994; Al-Dajani, 2016; Hameed et al., 2019). The Schneiderian membrane, which covers the inner part of the maxillary sinus cavity, is elevated to create space for guiding bone regeneration (Pjetursson and Lang, 2014). While spontaneous bone formation following sinus elevation has attracted considerable research attention, the precise role of the Schneiderian membrane in endosinus bone augmentation remains controversial (Dragonas et al., 2020).

Conflicting evidence exists regarding the osteoinductive potential of this membrane. Several studies concluded that endosinus new bone tissue was present near the elevated Schneiderian membrane, indicating that the Schneiderian membrane, with its osteoinductive potential, may contribute to bone augmentation (Palma et al., 2006; Moon et al., 2014; Rong et al., 2015). Conversely, Scala et al. (2010) reported that the Schneiderian membrane did not participate in new bone formation during healing events. The rabbit

✉ Misi SI, misi_si@zju.edu.cn
Mengfei YU, yumengfei@zju.edu.cn
* The two authors contributed equally to this work
Misi SI, https://orcid.org/0000-0001-5352-2046
Mengfei YU, https://orcid.org/0000-0002-7700-4697

Received Dec. 2, 2024; Revision accepted Mar. 19, 2025;
Crosschecked Apr. 23, 2026; Published online May 8, 2026

model has been extensively used to study bone healing processes after MSFE, owing to the species' anatomically favorable maxillary sinus characteristics that permit adequate space for bone formation (Asai et al., 2002; Yin et al., 2019; de Carvalho Silva Leocádio et al., 2021; Lee et al., 2022). Therefore, we used a rabbit MSFE model to further explore the contribution of the Schneiderian membrane in bone augmentation.

The mechanisms underlying bone regeneration following sinus elevation remain incompletely understood. Emerging evidence has shown that Schneiderian membrane-derived mesenchymal stem cells (SMMSCs) possess the ability for osteogenic, adipogenic, and chondrogenic differentiation (Wang et al., 2022). These cells exhibited characteristic mesenchymal markers (*STRO-1*, cluster of differentiation 146 (*CD146*), *CD29*, and *CD44*) and demonstrated functional similarities to other mesenchymal stem cell (MSC) populations (Srouji et al., 2009; Guo et al., 2015). Recent investigations have identified that $CD171^{+}/CD90^{+}$ MSCs derived from lamina propria had stronger proliferative capacity, while $CD171^{-}/CD90^{+}$ MSCs in the periosteal layer showed better osteogenic ability (Lv et al., 2024). Notably, Weng et al. (2022) identified the $Krt14^{+}Ctsk^{+}$ subset of cells in the Schneiderian membrane that robustly contributed to maxillofacial bone regeneration in mice, which displayed both epithelial and mesenchymal properties. The above studies demonstrated that the epithelial layer, lamina propria, and periosteal layer may have certain osteogenic potential. SMMSCs with specific molecular markers may be an important source of endogenous bone gain in the maxillary sinus. Thus, it is desirable to further characterize SMMSCs involved in new bone formation in the maxillary sinus.

Isolated from various tissues and organs, MSCs are excellent candidates for cell therapy in tissue regeneration (Granchi et al., 2010; Lemos et al., 2015; Fujii et al., 2023). Bone marrow-derived mesenchymal stem cells (BMSCs) have been reported as practical seed cells for bone regeneration (Granchi et al., 2010; Xie et al., 2022; Lee et al., 2023). However, allogeneic SMMSC transplantation has not been reported. Whether SMMSC could be suitable candidate for stem cell-based tissue engineering has not been examined. Therefore, we employed a well-established rabbit calvarial defect model to evaluate the bone regenerative capacity of scaffold-seeded SMMSCs (Saha et al., 2019; Liu et al., 2020).

In this study, we aimed to provide further evidence for the osteogenic capacity of the Schneiderian membrane and to characterize specific MSC subpopulations involved in sinus osteogenesis. We also aimed to assess the in vivo bone regenerative potential of allogeneic SMMSCs through calvarial defect repair and to provide new biological information on allogeneic SMMSC transplantation. To our knowledge, this represents the first comparative investigation of SMMSCs versus BMSCs in bone regeneration models. We hypothesize that the Schneiderian membrane contains clinically relevant MSC populations with regenerative potential equivalent to established MSC sources, potentially offering new avenues for tissue engineering applications.

2 Materials and methods

2.1 Single-cell RNA sequencing library preparation and data analysis

Fresh human Schneiderian membrane samples were preserved at 4 °C in tissue preservation solution. Sequencing was provided by OE Biotech Co., Ltd. (Shanghai, China). Briefly, cellular suspensions were loaded on the 10× Genomics Controller Single Cell Sequencer according to the manufacturer's protocol. Single-cell sequencing libraries were generated using the 10× Genomics Chromium Next GEM Single Cell 3' Reagent Kits (version 3.1). FASTQ files were processed and aligned to the GRCh38 human reference genome using Cell Ranger software (version 5.0.0). The unique molecular identifier (UMI) count matrix was analyzed using the Seurat R package (version 4.0.0). Cells were filtered based on gene numbers, UMI, and mitochondrial/hemoglobin RNA percentages. Doublets were identified using the DoubletFinder package (version 2.0.3). Principal-component analysis and graph-based clustering were performed. Cells were visualized using Uniform Manifold Approximation and Projection (UMAP). Marker genes and differentially expressed genes were identified using FindAllMarkers and FindMarkers functions (test.use=presto). $P<0.05$ and $|\log_2(\text{fold change})|>0.58$ were set as the threshold for significant differential expression. Detailed filtering criteria and analysis parameters are provided in Method S1.

2.2 Management of animals

Eighteen male New Zealand white rabbits (mean body weight 3.0 kg) were allocated to five experimental cohorts: baseline histological analysis (n=1); BMSC and SMMSC isolation for phenotypic characterization (n=3); in vivo cell tracking (n=3); bilateral MSFE with immunohistochemistry (n=2); and calvarial defect model (n=9). During the experimental period, the rabbits were kept individually in cages under standard laboratory conditions, with a standard diet and free access to water.

2.3 MSC isolation, culture, and tri-lineage induction

SMMSCs were isolated from the Schneiderian membrane by enzymatic digestion with collagenase I (3 mg/mL; Gibco, Thermo Fisher Scientific) for 1 h at 37 ℃. After neutralization, cells were collected by centrifugation, resuspended, and plated in α-minimal essential medium (α-MEM) with 10% (volume fraction) fetal bovine serum (FBS) and 1% (volume fraction) penicillin-streptomycin. BMSCs were harvested from the same rabbit as previously described (Saha et al., 2019). All cultures were maintained at 37 ℃ in 5% CO_2. The third passage of cells was used in subsequent experiments.

SMMSCs and BMSCs were isolated from three rabbits by density gradient centrifugation. Standardized fibroblast colony-forming unit (CFU-F) assays were conducted on passage 1 (P1) cells plated at 100 cells/cm^2 in α-MEM with 10% FBS. After 4 d, colonies were stained with crystal violet.

For trilineage differentiation, passage 2 (P2) SMMSCs were seeded in six-well plates at 1×10^4 cells/well. Osteogenic differentiation was induced with β-glycerophosphate, L-ascorbic acid, and dexamethasone for 21 d, and assessed by Alizarin Red S staining. Adipogenic differentiation was induced with insulin, dexamethasone, IBMX, and indomethacin for 21 d, and assessed by Oil Red O staining. Chondrogenic differentiation was induced with transforming growth factor-β1 (TGF-β1), vitamin C, dexamethasone, and pyruvate for 21 d, and assessed by Alcian Blue staining. Detailed medium compositions are provided in Method S2.

2.4 Immunofluorescence assay

After 21 d of differentiation, cells were fixed with 4% (40 g/L) paraformaldehyde (PFA), permeabilized with 0.5% (volume fraction) Triton X-100, blocked with 2% (20 g/L) bovine serum albumin (BSA), and incubated with primary antibodies against osteopontin (OPN), adiponectin (AND), and collagen type 2A (COL-II) overnight at 4 ℃, followed by fluorescence-conjugated secondary antibodies. Nuclear staining was performed with 4',6-diamidino-2-phenylindole (DAPI). Images were acquired using confocal fluorescence microscope (LSM980, Zeiss).

For paired-related homeobox 1 (PRRX1) immunohistochemistry, 4-μm paraffin sections of human and rabbit tissues were subjected to antigen retrieval, blocked with goat serum, and incubated with anti-PRRX1 overnight at 4 ℃, followed by donkey anti-goat Alexa Fluor 488. Sections were mounted with DAPI and imaged as above. Antibody dilutions are provided in Method S3.

2.5 Cytoskeleton staining

SMMSCs and BMSCs (2×10^6 cells) were seeded on gelatin methacryloyl (GelMA) scaffolds and incubated for 24 h. Cell scaffolds were fixed with 4% PFA, permeabilized with 0.5% Triton X-100, stained with rhodamine phalloidin and DAPI, and imaged by confocal microscope.

2.6 Surgical procedure

2.6.1 Rabbit sinus floor elevation model

Under general and local anesthesia, bilateral sinus floor elevation was performed. Two bone windows were created with a 4-mm diamond burr, and the Schneiderian membrane was elevated. Using a split-mouth design, the left sinus was filled with Bio-Oss® collagenated bone mineral and the right sinus with 5% (0.05 g/mL) GelMA hydrogel. A biodegradable collagen membrane (BioGide) was placed over the surgical field. Rabbits received postoperative penicillin and were sacrificed at 6 or 12 months.

2.6.2 Rabbit cranial bone defect model

Nine rabbits received four bilateral calvarial defects (8 mm diameter, 2 mm depth). Defects were randomly allocated to: (1) acellular GelMA scaffold; (2) SMMSC-loaded GelMA (2×10^6 cells); (3) BMSC-loaded GelMA (2×10^6 cells); or (4) untreated control. All defects were covered with a BioGide membrane. Animals were euthanized at 1, 2, and 3 months (n=3 per time point). Detailed surgical protocols are provided in Method S4.

2.7 CM-Dil tissue-labeling

Chloromethyl-benzamidodialkylcarbocyanine (CM-Dil) (1 g/L in ethanol) was diluted to 0.5 g/L with α-MEM containing 10% FBS and injected into the elevated Schneiderian membrane. Rabbits were sacrificed at 0, 4, and 8 weeks after surgery. Tissues were fixed, decalcified, embedded in O.C.T., sectioned (8 μm), and imaged by confocal microscope.

2.8 Micro-CT scanning

Fixed bone specimens were scanned with a micro-computed tomography (micro-CT) system (Milabs, Utrecht, Netherlands, U-CT-XUHR) at 55 kV, 455 μA, and 14.8 μm resolution. Three-dimensional (3D) images were reconstructed, and bone volume/total volume (BV/TV), trabecular thickness (Tb.Th), and trabecular spacing (Tb.Sp) were analyzed using Imalytics Preclinical version 2.1 (Gremse-IT GmbH, Aachen, Germany).

2.9 Histological observation

After micro-CT, specimens were decalcified in 10% (100 g/L) ethylenediaminetetraacetic acid (EDTA), embedded in paraffin, sectioned at 5 μm, and stained with hematoxylin and eosin (H&E). New bone area was analyzed using ImageJ (National Institutes of Health, Bethesda, Maryland, USA).

2.10 Statistical analysis

Data are presented as mean±standard deviation (SD). Comparisons between two groups were performed using two-tailed Student's *t*-test, and comparisons among multiple groups by one-way analysis of variance (ANOVA) (SPSS v19.0). $P<0.05$ was considered statistically significant.

3 Results

All rabbits recovered from anesthesia and the surgical procedure, and the sutures healed well. The rabbits did not show any signs of inflammation or infection by the time of sacrifice.

3.1 Schneiderian membrane's osteogenic potential in sinus augmentation models

Representative images of the rabbit sinus floor elevation model are shown in Fig. 1a. CM-Dil was further used to trace cells from the rabbit Schneiderian membrane and their progeny to identify the contribution of the membrane to bone regeneration (Fig. 1b). After four weeks, labeled cells underwent proliferation and increased significantly. After eight weeks, Dil-labeled cells gradually became widely distributed in the elevated region. Cells from the maxillary sinus membrane migrated, proliferated, and may have finally differentiated into osteogenic lineages in the elevated area. In the H&E-stained decalcified sample sections (Fig. 1c), new bone was repositioned near the elevated sinus membrane after a long period in two groups. We found that in the 6th month, the Bio-Oss group showed early calcified bone formation in the upper transplantation area near the Schneiderian membrane and around the bone graft material. In the GelMA hydrogel group, calcified tissue was scattered near the Schneiderian membrane and at the edge of the transplantation area. After 12 months of transplantation, a large amount of new bone tissue was formed near the Schneiderian membrane in both the Bio-Oss and GelMA hydrogel groups, with a further calcified portion. Active osteoblast aggregation was observed under the Schneiderian membrane, which indicated that the membrane may have long-term bone-inducing potential. Taking these findings together, our data suggested that the maxillary sinus membrane may directly participate in de novo bone regeneration in the rabbit maxillary sinus augmentation model.

The morphological observations revealed that the rabbit Schneiderian membrane was composed of three layers: the epithelium, lamina propria, and periosteum (Figs. S1a and S1b). The upper cortex was composed of a false multilayered epithelium with a neatly arranged ciliated structure. The lamina propria layer was rich in maxillary sinus glands and collagen fibers, and the periosteum layer was closely connected with the bone wall. A recent study suggested that the lamina propria layer and the periosteum layer of the human Schneiderian membrane contained two types of MSCs (Lv et al., 2024), which may explain the osteogenic potential of the Schneiderian membrane.

3.2 Identification of SMMSCs by single-cell RNA sequencing

To identify the cell subsets, distinct populations were identified, including 1 cluster for mesenchymal cells, 5 clusters for globose basal cells, 3 clusters for airway basal cells, 1 cluster for endothelial cells, 2 clusters for secretory goblet cells, 6 clusters for ciliated

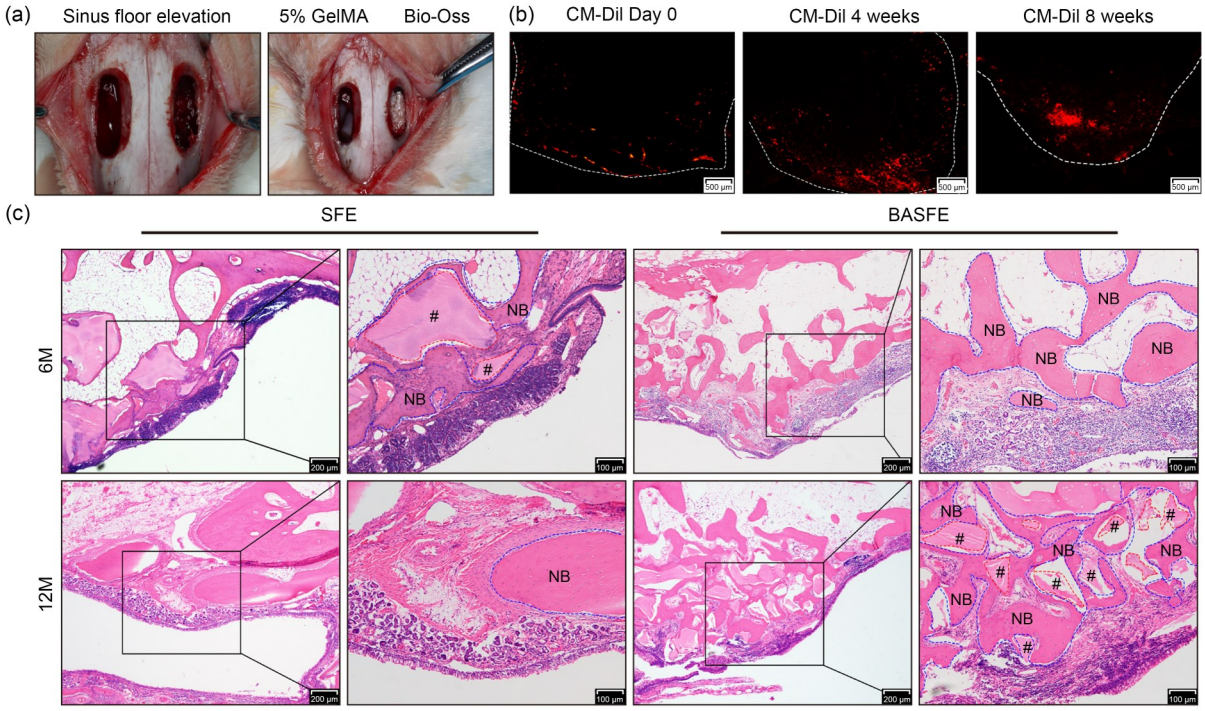

Fig. 1 Schneiderian membrane participated in endosinus bone formation in the rabbit sinus floor elevation model. (a) Procedure of rabbit sinus floor elevation. The bony windows were obtained by surgery, frontal view. Elevated spaces of the two sinuses were filled with Bio-Oss and 5% (volume fraction) gelatin methacryloyl (GelMA)-based hydrogels, respectively. (b) Chloromethyl-benzamidodialkylcarbocyanine (CM-Dil) was used to evaluate the contribution of the Schneiderian membrane to endosinus bone formation. With the extension of tracing time, cells derived from the Schneiderian membrane gradually proliferated. Dotted lines mark the elevated Schneiderian membrane, below which is the maxillary sinus cavity. (c) Representative histological images of hematoxylin and eosin (H&E) staining at 6 months (6M) and 12 months (12M) of two groups. New bone (NB) was located near the elevated Schneiderian membrane. The right image of each pair shows a magnified rectangular region of the left image. Blue dotted lines mark NB, red dotted lines and # mark unabsorbed grafting materials. SFE: sinus floor elevation; BASFE: bone-added sinus floor elevation.

cells, 1 cluster for monocytes, and 1 cluster for lymphocytes (Figs. 2a and 2b). Briefly, globose basal cells expressed KH RNA-binding domain-containing, signal transduction-associated 2 (*KHDRBS2*), tumor protein P63 (*TP63*), and transmembrane and tetratricopeptide repeat-containing 1 (*TMTC1*), while endothelial cells showed specific expression of endomucin (*EMCN*), von Willebrand factor (*vMF*), and LIM domain-binding 2 (*LDB2*). Significantly elevated levels of *AL139815.1*, cilia and flagella-associated protein 157 (*CFAP157*), and *AC137810.1* were used to distinguish the ciliated cells, and the expression levels of regulating synaptic membrane exocytosis 1 (*RIMS1*), limbic system-associated membrane protein (*LSAMP*), and *AC092691.1* were used to distinguish secretory goblet cells. Monocytes and lymphocytes expressed high levels of engulfment and cell motility 1 (*ELMO1*), Rho GTPase activating protein 15 (*ARHGAP15*), protein tyrosine phosphatase receptor type C (*PTPRC*), and *AC079793.1*. Mesenchymal cells showed high levels of *PRRX1*, zinc finger E-box-binding homeobox 1 (*ZEB1*), and neuron navigator 3 (*NAV3*). We further observed that cluster 9 was highly enriched in the previously reported mesenchymal marker *PRRX1* (Fig. 2c). Specifically, *PRRX1* was also identified as a classical MSC marker in the maxillofacial region. We found that *PRRX1*$^+$ MSCs could be divided into five subclusters (Figs. S2a and S2b). Besides, the pseudotime differentiation trajectory (Fig. S2c) indicated that different *PRRX1*$^+$ MSC subclusters may have different osteogenic differentiation capacities.

Through immunofluorescence (IF) staining, we further revealed the localization of *PRRX1*$^+$ cells in human and rabbit Schneiderian membranes. As shown in Figs. 2d and 2e, *PRRX1*$^+$ cells were scattered in the lamina propria layer in both human and rabbit Schneiderian membranes, close to the periosteum layer. After sinus floor elevation for four weeks, *PRRX1*$^+$

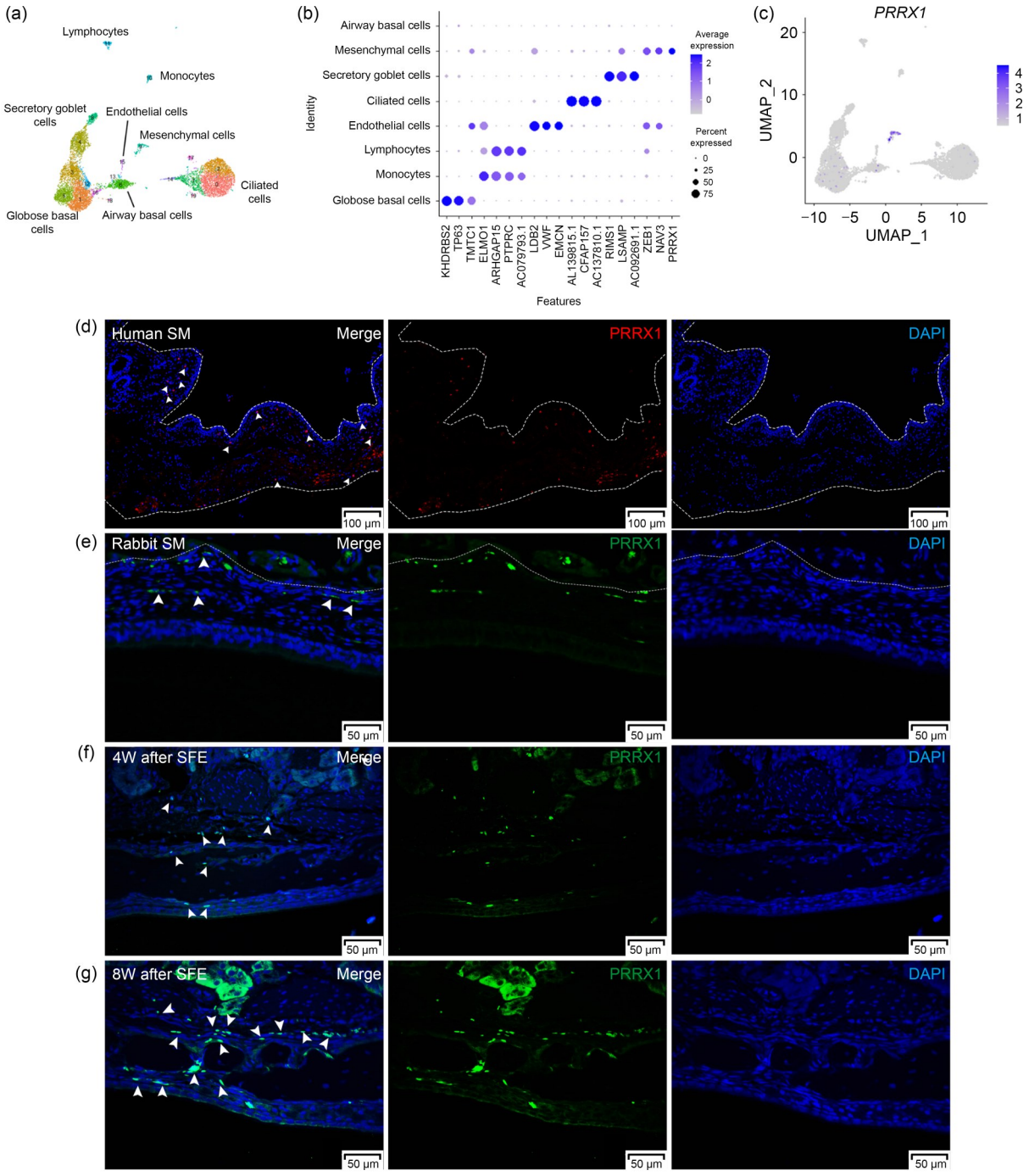

Fig. 2 Features of paired-related homeobox 1 (*PRRX1*$^+$) cells in the Schneiderian membrane. (a) A transcriptomic map of cells in the human maxillary sinus membrane produced by single-cell RNA sequencing, with cell type annotations of distinct clusters. (b) The average expression levels of key markers for different types of cells, as well as the percentage of cells expressing each marker. (c) A Uniform Manifold Approximation and Projection (UMAP) plot of mesenchymal cells based on their marker gene *PRRX1*. (d) *PRRX1*$^+$ cells were detected by immunofluorescent staining in the human Schneiderian membrane. The dotted lines mark the Schneiderian membrane and the maxillary bone. The arrowheads mark the *PRRX1*$^+$ cells in the human Schneiderian membrane. (e) *PRRX1*$^+$ cells were detected by immunofluorescent staining in the rabbit Schneiderian membrane. The dotted lines mark the Schneiderian membrane, above which is the maxillary bone. The arrowheads mark *PRRX1*$^+$ cells in the rabbit Schneiderian membrane. (f, g) *PRRX1*$^+$ cells were identified by immunofluorescent staining at 4 weeks (4W) and 8 weeks (8W) after sinus floor elevation (SFE) surgery, with arrowheads marking *PRRX1*$^+$ cells in the new bone. SM: Schneiderian membrane; DAPI: 4',6-diamidino-2-phenylindole; SFE: sinus floor elevation.

cells proliferated and participated in the early stage of new bone formation (Fig. 2f). After eight weeks, more *PRRX1*$^+$ cells appeared in the elevated zone, suggesting that *PRRX1*$^+$ cells may further promote bone regeneration (Fig. 2g). Building upon integrative analysis of single-cell RNA sequencing and spatially resolved IF staining data, our findings suggested that *PRRX1*$^+$ cell populations localized within both the lamina propria and periosteal compartments could represent progenitor lineages potentially associated with endosinus osteogenic processes.

3.3 Characterization and differentiation potential of rabbit SMMSCs

Primary cultured SMMSCs showed spindle-shaped fibroblast-like morphology, similar to the cultures of MSCs derived from other tissues (Fig. 3a). A CFU-F assay was conducted on P1 rabbit SMMSCs and BMSCs to identify their self-renewal ability. Fig. 3b shows representative colonies after cultivating rabbit SMMSCs and BMSCs for 2 d. SMMSCs showed significantly higher self-renewal ability than BMSCs (P<0.05).

The capacity of rabbit SMMSCs to differentiate into osteogenic, adipogenic, and chondrogenic cells was investigated under in vitro conditions. For osteogenic differentiation, Alizarin Red S staining revealed rabbit SMMSCs differentiated into osteoblasts after 21 d of induction (Fig. 3c). These observations were supported by positive OPN staining detected in osteogenic rabbit SMMSCs (Fig. 3d). Adipogenic SMMSCs were stained with Oil Red O to assess lipid droplets (Fig. 3e). The adipogenic marker ADN evaluated by IF was significantly upregulated in adipogenic SMMSCs (Fig. 3f). For chondrogenic differentiation, the pellet cultures stained by Alcian Blue revealed that chondrogenic rabbit SMMSCs increased after 21 d of chondrogenic induction (Fig. 3g). The IF experiment also showed that COL-II significantly increased in chondrogenic rabbit SMMSCs (Fig. 3h). Taken together, these results showed that rabbit SMMSCs had a better self-renewal capability than BMSCs, and had the potential to form osteogenic, adipogenic, and chondrogenic lineage cells.

3.4 Osteogenic potential of rabbit SMMSCs in cranial defect repair

Cytoskeleton staining indicated that the GelMA-based scaffold supported the expansion of SMMSCs and BMSCs (Fig. 4a). Representative images of the rabbit cranial bone defect model are shown in Fig. 4b. Fig. 4c depicts micro-CT 3D images of cranial bone defects taken at 1, 2, and 3 months following: no treatment; implantation with GelMA-based scaffolds only; rabbit SMMSCs/GelMA-based scaffolds; rabbit BMSCs/GelMA-based scaffolds. At one month post-operatively, new bone formation was clearly observed at the edge and center of the cranial defects in the SMMSCs and BMSCs groups, while only a small amount of new bone formation was observed at the edge of the cranial defect in the blank control group and the GelMA group. The BV/TV was significantly higher in the SMMSCs/GelMA-based scaffold group than in the BMSCs/GelMA-based scaffold group (P< 0.01), the GelMA-based scaffold group (P<0.001), or the blank group (P<0.001) (Fig. 4d). In addition, the Tb.Th of new bone in the SMMSCs/GelMA-based scaffold group was significantly higher than that in the GelMA-based scaffold group (P<0.01) or the blank group (P<0.001). These results indicated that SMMSCs had better bone defect repair capacity at an early stage than BMSCs.

As time progressed, the percentage of new bone formation increased in all groups. After two months, the SMMSCs/GelMA- and BMSCs/GelMA-based scaffold groups had mostly repaired the bone defect. At this time, a large defect was still visible in the center of the cranial bone in the GelMA-based scaffold and blank groups. After two months, the BV/TV in the SMMSCs/GelMA-based scaffold group was significantly higher than that in the GelMA-based scaffold group (P<0.05), and the BV/TV in the BMSCs/GelMA-based scaffold group was also significantly higher than that in the GelMA group (P<0.01) (Fig. 4d). The considerable new bone formation in the SMMSCs/GelMA- and BMSCs/GelMA-based scaffold groups had mostly repaired the defect, while, in contrast, the GelMA-based scaffold and blank control groups showed only a slight increase in newly formed bone. The bone defect had mostly healed in all groups after three months. After three months, the BV/TV in the BMSCs/GelMA-based scaffold group was significantly higher than those in the GelMA-based scaffold group (P<0.01) and the blank group (P<0.01), and Tb.Th in the BMSCs/GelMA-based scaffold group was significantly higher than that in blank group (P<0.05) (Fig. 4d). These results indicate that both SMMSCs and BMSCs have

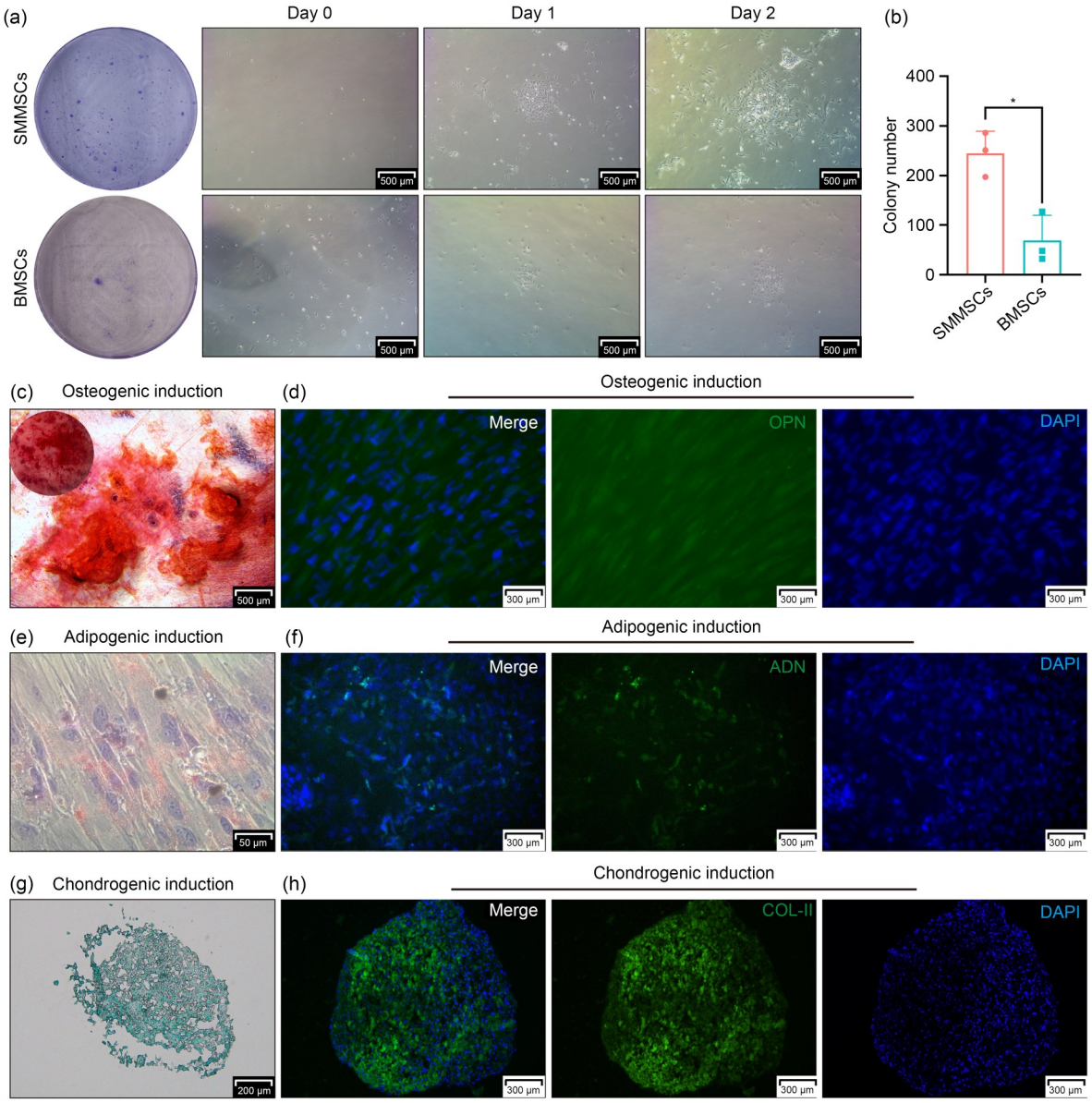

Fig. 3 Characterization of rabbit Schneiderian membrane-derived mesenchymal stem cells (SMMSCs). (a) Representative images of fibroblast colony-forming unit (CFU-F) after cultivating rabbit SMMSCs and bone marrow-derived mesenchymal stem cells (BMSCs) for 2 d under inverted microscopy. (b) SMMSCs showed better self-renewal ability than BMSCs. Differences between groups are expressed as mean±standard deviation (SD). n=3. * P<0.05, two-tailed Student's unpaired t-test. (c) Representative images of Alizarin Red S staining for rabbit SMMSC osteogenic differentiation. (d) Osteopontin (OPN) was determined by immunofluorescent staining. (e) Adipogenic rabbit SMMSCs stained by Oil Red O. (f) Adiponectin (ADN) was revealed by immunofluorescent staining. (g) Chondrogenic rabbit SMMSCs stained by Alcian Blue. (h) Collagen type 2A (COL-II) was identified by immunofluorescent staining. DAPI: 4',6-diamidino-2-phenylindole.

good bone repair ability, and SMMSCs may have better in vivo osteogenic ability than BMSCs at an early postoperative stage.

H&E staining of the cranial bone defects is shown in Fig. 5. After one month, in the GelMA-based scaffold and blank control groups, the center of defect sites was filled mostly with connective tissue rather than newly formed bone. Only minimal bone formation and a few bony islands were noted on the edge of the defects. On the other hand, the MSC-treated group showed considerable new bone formation: circular new bony islands with early woven bone were observed, originating from the periphery of defects. The SMMSCs/GelMA-based scaffold group formed more

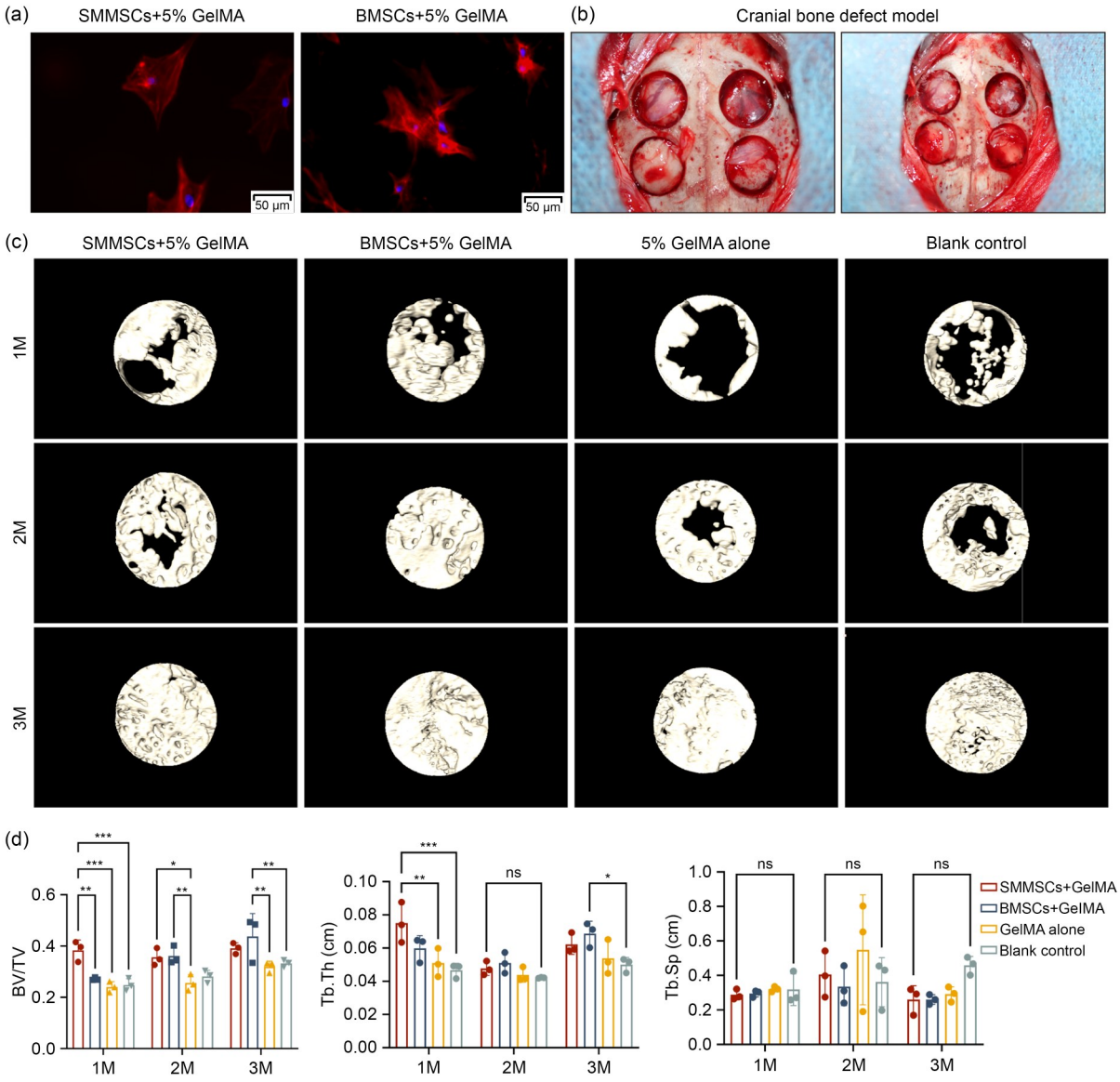

Fig. 4 Earlier bone formation by Schneiderian membrane-derived mesenchymal stem cells (SMMSCs) relative to bone marrow-derived mesenchymal stem cells (BMSCs) in calvarial defects. (a) Cytoskeleton staining was used to observe the growth of rabbit SMMSCs and BMSCs on gelatin methacryloyl (GelMA)-based scaffolds. (b) Rabbit cranial bone defect model, frontal view. (c) Representative 3-dimensional micro-computed tomography (micro-CT) images of a top view of the reconstructed rabbit calvaria at 1 month (1M), 2 months (2M), and 3 months (3M). Remarkable new bone formation was observed in the SMMSCs/GelMA- and BMSCs/GelMA-based scaffold groups at one month after surgery. (d) Morphometric analysis of bone volume/total volume (BV/TV), trabecular thickness (Tb.Th), and trabecular spacing (Tb.Sp) within calvarial defects at 1M, 2M, and 3M for different groups. Analysis of variance (ANOVA), followed by Tukey's post hoc test. Differences between groups are expressed as mean±standard deviation (SD). n=3. * P<0.05, ** P<0.01, *** P<0.001; ns: not significant.

continuous fibrous osteoid structures and bone marrow cavities, with a large number of osteoblasts and new bony islands.

After two months of healing, substantial bony ingrowth was observed and bone maturation was more extensive in the MSC-treated groups. Mature continuous lamellar bone as well as bone marrow cavities were noted in the SMMSCs/GelMA- and BMSCs/GelMA-based scaffold groups, while new bone formation was still limited in the blank and GelMA control groups, with a limited number of independent bone islands or discontinuous thin fibroid bone. After three months, robust bone regeneration and defect healing were clearly observed in the defects implanted

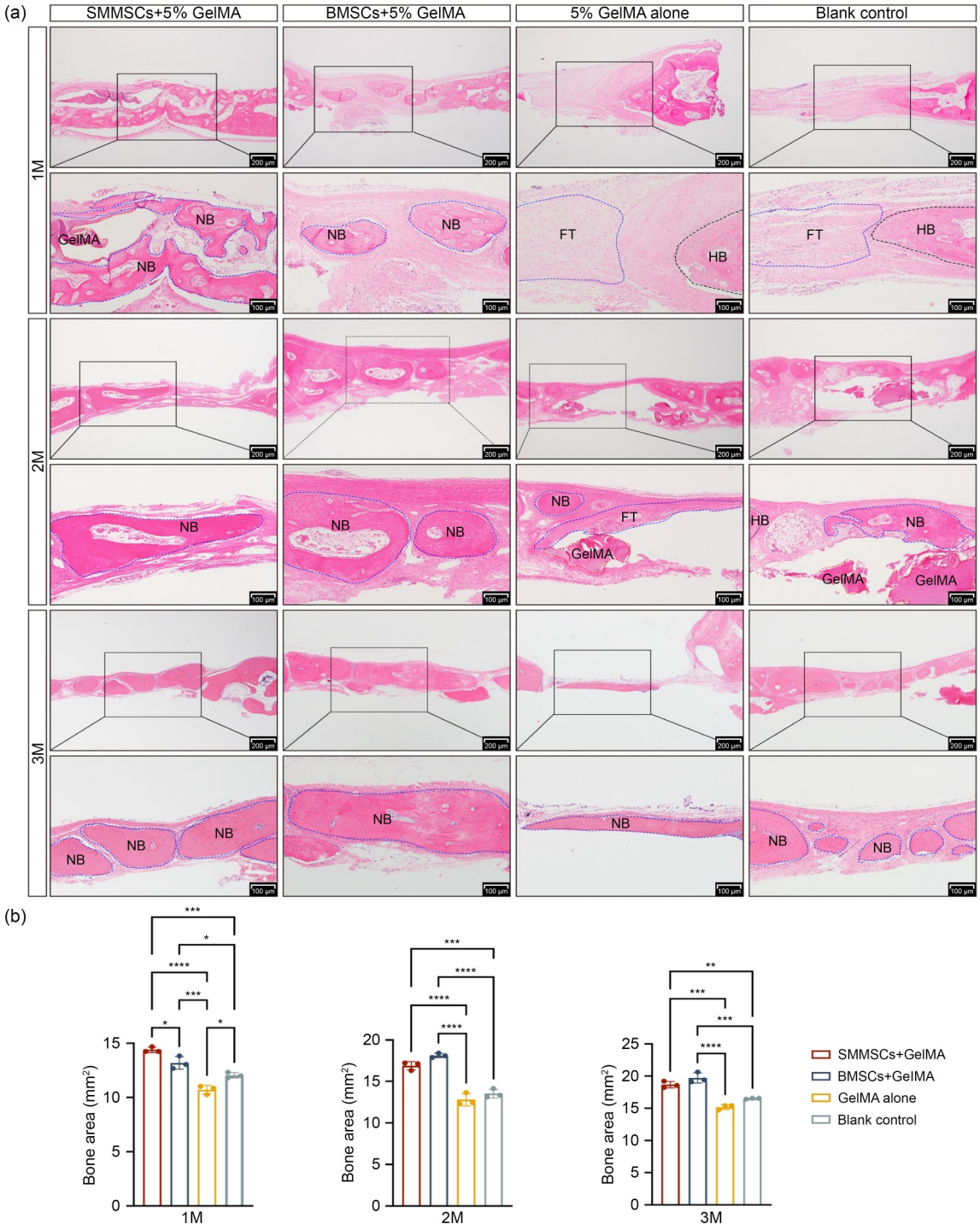

Fig. 5 Accelerated osteogenesis of Schneiderian membrane-derived mesenchymal stem cells (SMMSCs) versus bone marrow-derived mesenchymal stem cells (BMSCs) during early-stage calvarial healing. (a) Histomorphological detection was demonstrated by hematoxylin and eosin (H&E) staining at 1 month (1M), 2 months (2M), and 3 months (3M). Continuous new bone formation was detected in the SMMSCs/gelatin methacryloyl (GelMA)- and BMSCs/GelMA-based scaffold groups at different periods after surgery. The lower image in each set shows a magnified rectangular region of the upper image. Blue dotted lines mark the new bone (NB) and fibrous tissue (FT), the red dotted lines mark unabsorbed GelMA materials, and the black dotted lines mark the host bone (HB). (b) ImageJ was used to measure the bone formation area of each treatment group on the H&E-stained slides. Analysis of variance (ANOVA), followed by Tukey's post hoc test. Differences between groups are expressed as mean±standard deviation (SD). n=3. * P<0.05, ** P<0.01, *** P<0.001, **** P<0.0001.

with SMMSCs and BMSCs. The rabbit's cranium defect area was covered with thick mature lamellar bone junctions with large and orderly trabeculae in the SMMSCs/GelMA- and BMSCs/GelMA-based scaffold groups. In contrast, the blank and GelMA control groups formed isolated bone islands surrounded by fibrous tissue, with thin bone and small trabeculae.

A semiquantitative analysis of the bone formation in the cranial bone defects suggested that SMMSCs exhibited the highest healing speeds during the entire bone healing process. After one month, the proportion of new bone in the SMMSCs/GelMA-based scaffold group was significantly higher than that of the BMSCs/GelMA-based scaffold group (P<0.05), GelMA-based scaffold group (P<0.0001), and blank group (P<0.01) (Fig. 5b). The proportion of new bone in the BMSCs/GelMA-based scaffold group was significantly higher than that in the GelMA-based scaffold group (P<0.001) and the blank group (P<0.05). After two and three months, both SMMSCs and BMSCs significantly enhanced bone regeneration in the cranial bone defect model when compared with GelMA alone or the blank control (all P<0.05). These results suggest that both SMMSCs and BMSCs had the ability for bone regeneration in vivo, and that although both cell types achieved robust healing by three months, SMMSCs demonstrated a superior and faster osteogenic capacity during the early stage (one month) of bone defect repair.

4 Discussion

Vertical bone regeneration in the maxillary posterior alveolar ridge remains a significant clinical challenge for successful dental implant placement. Maxillary sinus elevation is usually performed in these cases. There is controversy regarding the underlying mechanism of osteogenesis in the maxillary sinus cavity. Previous studies suggested that bone regeneration after MSFE relied mainly on the activation of osteoprogenitor cells located in the maxillary bone wall and bone marrow (Scala et al., 2012; Jungner et al., 2015; Qian et al., 2018). In recent years, the Schneiderian membrane, which covers the maxillary sinus cavity, has attracted attention from scholars for inducing regenerative tissues. Guo et al. (2015) proposed that the Schneiderian membrane was one of the sources of osteoblasts involved in the endosinus bone remodeling process. Srouji et al. (2010) showed that when the sinus membrane was folded and transplanted in an ectopic subcutaneous location in nude mice, strong positive staining of alkaline phosphatase (ALP) appeared at the periosteum-like structure. Weng et al. (2022) showed that *Krt14*$^{+}$*Ctsk*$^{+}$ cells in the Schneiderian membrane contributed to maxillofacial bone osteogenesis and regeneration through dual recombinase-mediated lineage tracing. However, Scala et al. (2012) found no evidence that the Schneiderian membrane participated in new bone formation after MSFE in histological sections of primates. Lim et al. (2022) documented the early degradation of pseudo-periosteal structures during wound healing, postulating a limited osteogenic contribution from the sinus mucosa. This observation aligns with retrospective clinical evidence demonstrating enlargement of the maxillary sinus ostium post-augmentation (Guo et al., 2015; Makary et al., 2016; Sakuma et al., 2020), suggesting that chronic inflammatory processes and sustained edema may adversely affect neo-osteogenesis. Therefore, the mechanistic role of the sinus mucosa in endosinus osteogenesis warrants further experimental validation through integrated in situ cell lineage tagging and histomorphometric analysis.

In the present animal experiments, we performed maxillary sinus augmentation with Bio-Oss or GelMA hydrogel in rabbits for long-term observation. Bio-Oss is a standard commercial bone graft substitute for maxillary sinus floor augmentation (Pereira et al., 2024), and GelMA hydrogel has good biocompatibility and provides structural support (Chen and Tsai, 2025; Liu et al., 2025). After six months, both Bio-Oss materials and GelMA hydrogel were retained in the rabbit sinus as they could be seen clearly in H&E-stained slides. At 12 months post-surgery, GelMA hydrogel in the rabbit sinus had been resorbed to some extent and replaced by vital bone. Ingrowth of newly formed bone could be found around the implantation materials in both groups. Our results showed that the elevated Schneiderian membrane was in intimate contact with the new bone after a long period of time. To further explain the unique function of the sinus mucosa in the endosinus bone gain, CM-Dil tracing was used to track the Schneiderian membrane-derived cells after sinus elevation. The labeled cells proliferated and scattered in the maxillary sinus cavity in postoperative Weeks 4

and 8. We hypothesize that the de novo bone generated from the Schneiderian membrane may exhibit distinct histomorphometric characteristics, particularly in its preferential deposition along the arcuate superior region of the sinus compartment. This osteogenic pattern potentially diverges from the intramembranous ossification processes originating from the maxillary bony walls. The results indicated that the Schneiderian membrane-derived cells directly participated in bone gain after sinus lifting.

H&E and Masson trichrome-stained sections showed that the Schneiderian membrane was composed of the epithelial lining, lamina propria, and a periosteum-like structure. After the sinus membrane is elevated, the osteoprogenitor cells may be stimulated to start the osteogenesis process. Meanwhile, as a barrier membrane, the Schneiderian membrane could also protect the blood clot in the raised space, thereby contributing to the osteogenic response (Falah et al., 2016).

The cellular composition of the Schneiderian membrane is not well understood. Therefore, we conducted single-cell RNA sequencing to explain the contribution of the Schneiderian membrane and identify the MSCs residing within it. A similar single-cell sequencing-guided approach was recently employed by Hu et al. (2025) to identify disease-specific osteoblast subpopulations in osteoporotic niches, highlighting the power of this technology in revealing cell populations critical for bone regeneration. We determined the cellular hierarchy of the maxillary sinus membrane and identified specifically labeled MSCs. The human maxillary sinus membrane contains mesenchymal cells, globose basal cells, airway basal cells, endothelial cells, secretory goblet cells, ciliated cells, monocytes, and lymphocytes. In recent years, three distinct cell markers have been used to identify MSCs and skeletal stem cells in the craniofacial region, including *PRRX1* (Tooze et al., 2023), GLI family zinc finger 1 (*GLI1*) (Yu et al., 2021), and axis inhibition protein 2 (*AXIN2*) (di Pietro et al., 2020). *PRRX1*, which acts as a transcriptional co-activator, has been shown to be expressed within periosteal bone (Deng et al., 2019; Yang et al., 2022). *GLI1*$^+$ cells seem to be involved in cranial suture regeneration and bone homeostasis (Zhao et al., 2015; Yu et al., 2021). Finally, *AXIN2*$^+$ cells have been proposed to have long-term self-renewal and differentiation abilities during calvarial development (Maruyama et al., 2017). *PRRX1*, a lineage-specific subset of craniofacial mesenchyme progenitors, appears to contain osteoprogenitors in both human and rabbit Schneiderian membranes. After sinus floor elevation, *PRRX1*$^+$ MSCs scattered in both the lamina propria and periosteum layers were considered to play an important role in guiding bone regeneration. Once the sinus membrane was lifted, *PRRX1*$^+$ cells were enriched and located in the newly-formed bone, suggesting that they contributed to the development of newly formed bone tissue. Interestingly, *PRRX1*$^+$ MSCs could be further divided into five subpopulations, with pseudotime analyses showing their differentiation trajectories. The heterogeneity and hierarchy of *PRRX1*$^+$ MSC subpopulations that participate in endosinus bone regeneration and their specific function will be verified in further studies. While preliminary findings suggest *PRRX1*$^+$ SMMSCs' involvement in sinus bone formation, the current study had limitations in conclusively demonstrating cellular dynamics and commitment pathways. Definitive validation requires implementation of Cre-*loxP*-based lineage tracing in transgenic models coupled with single-cell transcriptomic profiling, which may permit high-resolution tracking of *PRRX1*$^+$ progenitor differentiation trajectories during osteogenic processes.

Numerous MSCs from different tissues have been extensively applied in cell therapies (Granchi et al., 2010; Lemos et al., 2015; Fujii et al., 2023). Cells isolated from various sources exhibit different biological characteristics (Sui et al., 2019). In particular, the bone marrow stromal cells and periosteum-derived cells have been the main sources used in bone repair and tissue engineering (Zhu et al., 2023). In the present study, SMMSCs fostered a fibroblast-like appearance. The colony-forming potential is one of the most essential characteristics of MSCs (Friedenstein et al., 1970). Our results showed that the self-renewal ability of SMMSCs was distinctly higher than that of BMSCs. In addition, MSCs are known for their capacity to differentiate into multi-lineages toward osteoblasts, adipocytes, and chondroblasts (Suchanecka et al., 2025). The multilineage differentiation potential of SMMSCs was proven by the positive staining of Alizarin Red S, Oil Red O, and Alcian Blue, as well as the elevated lineage-specific expression level, including OPN, ADN, and COL-II. Other researchers also derived MSCs from the human Schneiderian membrane that were committed to the osteogenic lineage (Guo et al., 2015). Some research groups have provided evidence that SMMSCs express

the stem cell marker *STRO-1* and the microvascular mesenchymal progenitor marker *CD146*, reconfirming the presence of a progenitor cell population in the Schneiderian membrane (Derjac-Aramă et al., 2015; Guo et al., 2015).

Hence, SMMSCs are a population of MSCs with high self-renewal capability and multi-lineage differentiation potential, which may exhibit significant effects in tissue-engineered bone formation after maxillary sinus floor augmentation. These results emphasize the high bone regeneration potential of MSCs derived from the Schneiderian membrane and raise the possibility of their use in an MSC-based therapeutic therapy against bone defects in vivo.

The cranial bone defect model has been widely used to investigate the effects of different MSC-based treatment modalities (Saha et al., 2019; Liu et al., 2020). By placing collagen membranes as barriers, we prevented the ingrowth of fibrous connective tissues during the healing process. The transplant cell-based scaffolds were the main source of bone regeneration (Maurer et al., 2018). With high osteogenic potential, BMSCs have been widely used in many tissue engineering studies (Granchi et al., 2010; Xie et al., 2022; Lee et al., 2023). Thus, we used BMSCs as a control to evaluate the bone regeneration potential of SMMSCs. We observed active new bone formation as well as osteoid/ossifying mesenchyme in SMMSCs/GelMA-based scaffolds in the first four weeks of healing. On the other hand, only small amounts of new bony islands were observed in BMSCs/GelMA-based scaffolds. Note that we found significantly higher BV/TV values in the SMMSCs/GelMA-based scaffold group than in the BMSCs/GelMA-based scaffold group. The other two groups promoted only minimal new bone in the margin area, as the center of the defect regions was filled with connective tissues but not trabecular bone. At eight weeks after surgery, both the BMSCs/GelMA-based and SMMSCs/GelMA-based scaffold groups showed well-organized mature bone with marrow space filled with fat cells. Continuous cortical bone was observed in all four groups after 12 weeks. Compared with the control groups, MSC-treated groups showed a better degree of mineralization and thicker cortical bone. In conclusion, the results of the present study suggest that more pronounced bone formation occurred in the SMMSCs/GelMA-based scaffold group in the early healing stage beyond four weeks. SMMSCs may have superior osteogenic differentiation and mineralization abilities than BMSCs during the initial period of bone healing in vivo. To reduce individual differences, we did not use a critical calvarial defect model in rabbits, and thus caution is necessary when considering the statistical results. To our knowledge, this is the first study to evaluate the in vivo osteogenesis efficacy of SMMSCs in a rabbit calvarial defect model. When compared with autografts, allografts, and xenografts for bone regeneration, allogeneic SMMSCs may have several advantages. This strategy could reduce the risk of immune rejection (Reinders et al., 2013; Ankrum et al., 2014; Chen et al., 2021), and SMMSCs could be isolated minimally invasively in a sinus floor elevation model. The GelMA scaffold used in this study could potentially be further optimized using strategies such as those reported by Ma et al. (2025), who incorporated silk fibroin and polyethylene oxide to enhance mechanical strength while maintaining biocompatibility. The comparative analysis revealed a paradoxical temporal divergence in osteogenic efficacy between SMMSCs and BMSCs, with SMMSCs showing superior early-stage osteoinductive capacity in the cranial defect model. This differential performance profile likely stems from intrinsic cellular adaptations to their respective tissue niches. The observed spatial patterning of de novo bone formation, particularly the peripheral-to-central mineralization gradient in augmented sinuses, may align with the demonstrated propensity of SMMSCs for early bone regeneration. We hypothesize that, as mucosal-derived cells subjected to cyclic respiratory deformation, SMMSCs may have enhanced capacity to transduce compressive stresses into pro-osteogenic biochemical signals after sinus floor elevation.

This study's conclusions must be interpreted with regard to its methodological constraints. Although CM-Dil tracing indicated maxillary sinus membrane involvement in osteogenesis within the rabbit model, direct clinical extrapolation remains problematic due to significant anatomical and physiological disparities in Schneiderian membrane morphology and sinus augmentation dynamics between the species. Moreover, the distinct biological microenvironment of calvarial defects compared to sinus elevation sites underscores the need for caution when translating these findings to maxillofacial regeneration scenarios. Further investigations using human-derived models and clinical

correlation studies are imperative to elucidate the role of SMMSCs in human sinus floor elevation.

In this perspective, endosinus' new bone formation may promote the participation of the Schneiderian membrane in bone formation. Our study provides initial experimental evidence that the addition of the SMMSC transplant resembles a biologically active osteoinductive augmentation method, which may enhance new bone formation, especially in early bone healing. The demonstrated self-renewal capacity and multipotent differentiation potential of SMMSCs, particularly their osteogenic competency in both in vitro and in vivo models, position these cells as promising candidates for MSC-based regenerative approaches. To advance clinical translation, ongoing investigations focused on three critical aspects are currently underway: (1) ontogenetic characterization of SMMSC subpopulations; (2) mechanistic studies of their paracrine signaling in 3D sinus augmentation environments; and (3) development of human-relevant experimental models to validate their osteoinductive capacity in maxillofacial regeneration scenarios.

5 Conclusions

Histological and immunohistochemical evidence suggested that the Schneiderian membrane may act as a cellular reservoir supporting osseointegration post-sinus augmentation, though definitive validation via lineage-tracing and spatial transcriptomics is needed. SMMSC transplantation enhanced earlier calvarial bone regeneration compared to BMSCs. Given their robust self-renewal and osteogenic potential in vitro and in vivo, SMMSCs may represent promising MSC-based therapeutic candidates for bone repair. Further investigations into their cellular origins and heterogeneity are underway.

Data availability statement

All data supporting the conclusions of the present study are included within this article.

Acknowledgments

This work was supported by the National Key Research and Development Program of China (No. 2023YFB3813003), the Innovative Talent of Zhejiang Provincial Health Commission, the Research and Development Project of Stomatology Hospital Zhejiang University School of Medicine (No. RD2023DLYB02), and the National Natural Science Foundation of China (No. 82430031).

Author contributions

Yuxin ZHAO performed the experiments, analyzed the data, and drafted and revised the manuscript. Jia WANG performed the experiments, and drafted and revised the manuscript. Dongqi YOU participated in the experiments. Yifan LU interpreted the data and prepared parts of the figures. Mengfei YU and Misi SI designed and supervised this study, and critically revised the manuscript. All authors have read and approved the final manuscript, and therefore, have full access to all the data in the study and take responsibility for the integrity and security of the data.

Compliance with ethics guidelines

Yuxin ZHAO, Jia WANG, Dongqi YOU, Yifan LU, Mengfei YU, and Misi SI declare that they have no conflicts of interest.

All procedures followed were in accordance with the ethical standards of the responsible committee on human experimentation (institutional and national) and with the 1964 Declaration of Helsinki and its later amendments or comparable ethical standards. Informed consent was obtained from all patients for being included in the study. Additional informed consent was obtained from all patients for whom identifying information is included in this article. Ethical approval for the human sample component of this study was obtained from the Ethics Committee of Stomatology Hospital, Zhejiang University School of Medicine, China (No. 2021-11). All animal experiments complied with the Animal Research Reporting In Vivo Experiments (ARRIVE) guidelines. The animal experiments were consented to by the Animal Care and Use Committee of Zhejiang University (No. ZJU20230115).

Declaration on the use of generative AI tools

No generative AI tools were used in the preparation of this manuscript.

References

Al-Dajani M, 2016. Recent trends in sinus lift surgery and their clinical implications. *Clin Implant Dent Relat Res*, 18(1):204-212. https://doi.org/10.1111/cid.12275

Ankrum JA, Ong JF, Karp JM, 2014. Mesenchymal stem cells: immune evasive, not immune privileged. *Nat Biotechnol*, 32(3):252-260. https://doi.org/10.1038/nbt.2816

Asai S, Shimizu Y, Ooya K, 2002. Maxillary sinus augmentation model in rabbits: effect of occluded nasal ostium on new bone formation. *Clin Oral Implants Res*, 13(4):405-409. https://doi.org/10.1034/j.1600-0501.2002.130409.x

Chen JM, Huang QY, Zhao YX, et al., 2021. The latest developments in immunomodulation of mesenchymal stem cells in the treatment of intrauterine adhesions, both allogeneic

and autologous. *Front Immunol*, 12:785717. https://doi.org/10.3389/fimmu.2021.785717

Chen PH, Tsai WB, 2025. Development of a photocrosslinkable collagen-bone matrix hydrogel for bone tissue engineering. *Polymers*, 17(7):935. https://doi.org/10.3390/polym17070935

de Carvalho Silva Leocádio A, Silva M, de Oliveira GJPL, et al., 2021. Osseointegration of different implant surfaces in areas grafted with deproteinized bovine bone associated or not with fresh bone marrow—preclinical study in rabbits. *Clin Oral Implants Res*, 32(6):767-775. https://doi.org/10.1111/clr.13746

Deng Q, Li P, Che MJ, et al., 2019. Activation of hedgehog signaling in mesenchymal stem cells induces cartilage and bone tumor formation via Wnt/β-Catenin. *eLife*, 8:e50208. https://doi.org/10.7554/eLife.50208

Derjac-Aramă AI, Sarafoleanu C, Manea CM, et al., 2015. Regenerative potential of human Schneiderian membrane: progenitor cells and epithelial-mesenchymal transition. *Anat Rec*, 298(12):2132-2140. https://doi.org/10.1002/ar.23276

di Pietro L, Barba M, Prampolini C, et al., 2020. GLI1 and AXIN2 are distinctive markers of human calvarial mesenchymal stromal cells in nonsyndromic craniosynostosis. *Int J Mol Sci*, 21(12):4356. https://doi.org/10.3390/ijms21124356

Dragonas P, Katsaros T, Schiavo J, et al., 2020. Osteogenic capacity of the sinus membrane following maxillary sinus augmentation procedures: a systematic review. *Int J Oral Implantol*, 13(3):213-232.

Falah M, Sohn DS, Srouji S, 2016. Graftless sinus augmentation with simultaneous dental implant placement: clinical results and biological perspectives. *Int J Oral Maxillofac Surg*, 45(9):1147-1153. https://doi.org/10.1016/j.ijom.2016.05.006

Friedenstein AJ, Chailakhjan RK, Lalykina KS, 1970. The development of fibroblast colonies in monolayer cultures of guinea-pig bone marrow and spleen cells. *Cell Proliferat*, 3(4):393-403. https://doi.org/10.1111/j.1365-2184.1970.tb00347.x

Fujii S, Takebe H, Mizoguchi T, et al., 2023. Bone formation ability of $Gli1^+$ cells in the periodontal ligament after tooth extraction. *Bone*, 173:116786. https://doi.org/10.1016/j.bone.2023.116786

Granchi D, Devescovi V, Baglio SR, et al., 2010. Biological basis for the use of autologous bone marrow stromal cells in the treatment of congenital pseudarthrosis of the tibia. *Bone*, 46(3):780-788. https://doi.org/10.1016/j.bone.2009.10.044

Guo JB, Weng JQ, Rong Q, et al., 2015. Investigation of multipotent postnatal stem cells from human maxillary sinus membrane. *Sci Rep*, 5:11660. https://doi.org/10.1038/srep11660

Hameed S, Bakhshalian N, Alwazan E, et al., 2019. Maxillary sinus floor and alveolar crest alterations following extraction of single maxillary molars: a retrospective cbct analysis. *Int J Periodontics Restorative Dent*, 39(4):545-551. https://doi.org/10.11607/prd.3865

Hu W, Fei TY, Liu ZC, et al., 2025. Single-cell RNA-sequencing-guided reactive oxygen species-scavenging hydrogel design for regeneration of osteoporotic bone. *J Zhejiang Univ-Sci B*, 26(12):1172-1191. https://doi.org/10.1631/jzus.B2500254

Jungner M, Cricchio G, Salata LA, et al., 2015. On the early mechanisms of bone formation after maxillary sinus membrane elevation: an experimental histological and immunohistochemical study. *Clin Implant Dent Relat Res*, 17(6):1092-1102. https://doi.org/10.1111/cid.12218

Lee E, Epanomeritakis IE, Lu V, et al., 2023. Bone marrow-derived mesenchymal stem cell implants for the treatment of focal chondral defects of the knee in animal models: a systematic review and meta-analysis. *Int J Mol Sci*, 24(4):3227. https://doi.org/10.3390/ijms24043227

Lee JY, Kim S, Shin SY, et al., 2022. Effectiveness of hydraulic pressure-assisted sinus augmentation in a rabbit sinus model: a preclinical study. *Clin Oral Investig*, 26(2):1581-1591. https://doi.org/10.1007/s00784-021-04131-z

Lemos DR, Eisner C, Hopkins CI, et al., 2015. Skeletal muscle-resident MSCs and bone formation. *Bone*, 80:19-23. https://doi.org/10.1016/j.bone.2015.06.013

Lim ST, Kusano K, Taniyama T, et al., 2022. Contribution to bone formation of the Schneiderian membrane after sinus augmentation: a histological study in rabbits. *Materials (Basel)*, 15(22):8077. https://doi.org/10.3390/ma15228077

Liu JQ, Kang J, Zou T, et al., 2025. Functional cobalt-doped hydrogel scaffold enhances concurrent vascularization and neurogenesis. *J Nanobiotechnol*, 23:179. https://doi.org/10.1186/s12951-025-03218-z

Liu YN, Wang HF, Dou HX, et al., 2020. Bone regeneration capacities of alveolar bone mesenchymal stem cells sheet in rabbit calvarial bone defect. *J Tissue Eng*, 11:1-12. https://doi.org/10.1177/2041731420930379

Lv HX, Xu J, Wang YH, et al., 2024. Isolation, identification and osteogenic capability analysis of mesenchymal stem cells derived from different layers of human maxillary sinus membrane. *J Clin Periodontol*, 51(6):754-765. https://doi.org/10.1111/jcpe.13956

Ma ZJ, Jia WD, Wang XY, et al., 2025. Novel multi-component synergistic bioink that balances biocompatibility and mechanical strength for cartilage regeneration. *J Zhejiang Univ-Sci B*, 26(12):1156-1171. https://doi.org/10.1631/jzus.B2500343

Makary C, Rebaudi A, Menhall A, et al., 2016. Changes in sinus membrane thickness after lateral sinus floor elevation: a radiographic study. *Int J Oral Maxillofac Implants*, 31(2):331-337. https://doi.org/10.11607/jomi.4108

Maruyama T, Jiang M, Abbott A, et al., 2017. Rap1b is an effector of Axin2 regulating crosstalk of signaling pathways during skeletal development. *J Bone Miner Res*, 32(9):1816-1828. https://doi.org/10.1002/jbmr.3171

Maurer T, Stoffel MH, Belyaev Y, et al., 2018. Structural characterization of four different naturally occurring porcine collagen membranes suitable for medical applications. *PLoS One*, 13(10):e0205027. https://doi.org/10.1371/journal.pone.0205027

Moon YS, Sohn DS, Moon JW, et al., 2014. Comparative histomorphometric analysis of maxillary sinus augmentation with absorbable collagen membrane and osteoinductive replaceable bony window in rabbits. *Implant Dent*, 23(1): 29-36. https://doi.org/10.1097/ID.0000000000000031

Palma VC, Magro-Filho O, de Oliveria JA, et al., 2006. Bone reformation and implant integration following maxillary sinus membrane elevation: an experimental study in primates. *Clin Implant Dent Relat Res*, 8(1):11-24. https://doi.org/10.2310/j.6480.2005.00026.x

Pereira RDS, de Carvalho MVNB, Hochuli-Vieira E, et al., 2024. Histomorphometric and micro-CT evaluation of cerabone and Bio-Oss in maxillary sinus lifting: a randomized clinical trial. *Medicina*, 60(11):1834. https://doi.org/10.3390/medicina60111834

Pjetursson BE, Lang NP, 2014. Sinus floor elevation utilizing the transalveolar approach. *Periodontol 2000*, 66(1):59-71. https://doi.org/10.1111/prd.12043

Qian SJ, Mo JJ, Shi JY, et al., 2018. Endo-sinus bone formation after transalveolar sinus floor elevation without grafting with simultaneous implant placement: histological and histomorphometric assessment in a dog model. *J Clin Periodontol*, 45(9):1118-1127. https://doi.org/10.1111/jcpe.12975

Reinders MEJ, de Fijter JW, Roelofs H, et al., 2013. Autologous bone marrow-derived mesenchymal stromal cells for the treatment of allograft rejection after renal transplantation: results of a phase I study. *Stem Cells Transl Med*, 2:107-111. https://doi.org/10.5966/sctm.2012-0114

Rong Q, Li X, Chen SL, et al., 2015. Effect of the Schneiderian membrane on the formation of bone after lifting the floor of the maxillary sinus: an experimental study in dogs. *Br J Oral Maxillofac Surg*, 53(7):607-612. https://doi.org/10.1016/j.bjoms.2015.02.010

Saha S, Yang XB, Wijayathunga N, et al., 2019. A biomimetic self-assembling peptide promotes bone regeneration in vivo: a rat cranial defect study. *Bone*, 127:602-611. https://doi.org/10.1016/j.bone.2019.06.020

Sakuma S, Ferri M, Imai H, et al., 2020. Involvement of the maxillary sinus ostium (MSO) in the edematous processes after sinus floor augmentation: a cone-beam computed tomographic study. *Int J Implant Dent*, 6:35. https://doi.org/10.1186/s40729-020-00233-7

Scala A, Botticelli D, Rangel IG, et al., 2010. Early healing after elevation of the maxillary sinus floor applying a lateral access: a histological study in monkeys. *Clin Oral Implants Res*, 21(12):1320-1326. https://doi.org/10.1111/j.1600-0501.2010.01964.x

Scala A, Botticelli D, Faeda RS, et al., 2012. Lack of influence of the Schneiderian membrane in forming new bone apical to implants simultaneously installed with sinus floor elevation: an experimental study in monkeys. *Clin Oral Implants Res*, 23(2):175-181. https://doi.org/10.1111/j.1600-0501.2011.02227.x

Srouji S, Kizhner T, Ben David D, et al., 2009. The Schneiderian membrane contains osteoprogenitor cells: in vivo and in vitro study. *Calcif Tissue Int*, 84(2):138-145. https://doi.org/10.1007/s00223-008-9202-x

Srouji S, Ben-David D, Lotan R, et al., 2010. The innate osteogenic potential of the maxillary sinus (Schneiderian) membrane: an ectopic tissue transplant model simulating sinus lifting. *Int J Oral Maxillofac Surg*, 39(8):793-801. https://doi.org/10.1016/j.ijom.2010.03.009

Suchanecka M, Grzelak J, Farzaneh M, et al., 2025. Adipose derived stem cells – sources, differentiation capacity and a new target for reconstructive and regenerative medicine. *Biomed Pharmacother*, 186:118036. https://doi.org/10.1016/j.biopha.2025.118036

Sui BD, Hu CH, Liu AQ, et al., 2019. Stem cell-based bone regeneration in diseased microenvironments: challenges and solutions. *Biomaterials*, 196:18-30. https://doi.org/10.1016/j.biomaterials.2017.10.046

Summers RB, 1994. A new concept in maxillary implant surgery: the osteotome technique. *Compendium*, 15(2):152, 154-156, 158.

Tatum H, 1986. Maxillary and sinus implant reconstructions. *Dent Clin North Am*, 30(2):207-229. https://doi.org/10.1016/S0011-8532(22)02107-3

Tooze RS, Miller KA, Swagemakers SMA, et al., 2023. Pathogenic variants in the paired-related homeobox 1 gene (PRRX1) cause craniosynostosis with incomplete penetrance. *Genet Med*, 25(9):100883. https://doi.org/10.1016/j.gim.2023.100883

Wang J, Sun Y, Liu YP, et al., 2022. Effects of platelet-rich fibrin on osteogenic differentiation of Schneiderian membrane derived mesenchymal stem cells and bone formation in maxillary sinus. *Cell Commun Signal*, 20:88. https://doi.org/10.1186/s12964-022-00844-0

Weng YT, Wang HC, Wu D, et al., 2022. A novel lineage of osteoprogenitor cells with dual epithelial and mesenchymal properties govern maxillofacial bone homeostasis and regeneration after MSFL. *Cell Res*, 32(9):814-830. https://doi.org/10.1038/s41422-022-00687-x

Xie C, Liang RJ, Ye JC, et al., 2022. High-efficient engineering of osteo-callus organoids for rapid bone regeneration within one month. *Biomaterials*, 288:121741. https://doi.org/10.1016/j.biomaterials.2022.121741

Yang CY, Li ZS, Liu Y, et al., 2022. Single-cell spatiotemporal analysis reveals cell fates and functions of transplanted mesenchymal stromal cells during bone repair. *Stem Cell Rep*, 17(10):2318-2333. https://doi.org/10.1016/j.stemcr.2022.08.008

Yin L, Zhou ZX, Shen M, et al., 2019. The human amniotic mesenchymal stem cells (hAMSCs) improve the implant osseointegration and bone regeneration in maxillary sinus floor elevation in rabbits. *Stem Cells Int*, 2019:9845497. https://doi.org/10.1155/2019/9845497

Yu MF, Ma L, Yuan Y, et al., 2021. Cranial suture regeneration mitigates skull and neurocognitive defects in craniosynostosis. *Cell*, 184 (1):243-256.e18.

https://doi.org/10.1016/j.cell.2020.11.037

Yuan Y, Loh YHE, Han X, et al., 2020. Spatiotemporal cellular movement and fate decisions during first pharyngeal arch morphogenesis. *Sci Adv*, 6(51):eabb0119. https://doi.org/10.1126/sciadv.abb0119

Zhao H, Feng JF, Ho TV, et al., 2015. The suture provides a niche for mesenchymal stem cells of craniofacial bones. *Nat Cell Biol*, 17(4):386-396. https://doi.org/10.1038/ncb3139

Zhu JX, Xiong JB, Ji W, 2023. A systematic review of bone marrow stromal cells and periosteum-derived cells for bone regeneration. *Tissue Eng Part B Rev*, 29(2):103-122. https://doi.org/10.1089/ten.TEB.2022.0115

Supplementary information

Figs. S1 and S2; Methods S1–S4